Rare Metal Materials and Engineering
Volume 52, Issue 2, February 2023
Available online at www.rmme.ac.cn

Science Press

Cite this article as: Wang Xingmao, Ding Yutian, Bi Zhongnan, et al. Dynamic Recrystallization Behavior of a Novel Ni-based Superalloy[J]. Rare Metal Materials and Engineering, 2023, 52(02): 517-526.

ARTICLE

Dynamic Recrystallization Behavior of a Novel Ni-based Superalloy

Wang Xingmao[1,2], Ding Yutian[1], Bi Zhongnan[2], Yu Hongyao[2], Du Jinhui[2], Gan Bin[2]

[1] State Key Laboratory of Advanced Processing and Recycling of Non-ferrous Metals, Lanzhou University of Technology, Lanzhou 730050, China; [2] Beijing Key Laboratory of Advanced High Temperature Materials, Central Iron and Steel Research Institute, Beijing 100081, China

Abstract: The dynamic recrystallization behavior of a novel Ni-based superalloy was investigated by means of isothermal compression tests in the temperature range of 1040–1120 °C, and the strain range of 0.35–1.2 with a strain rate of 0.1 s^{-1}. The microstructure evolution and nucleation mechanism of dynamic recrystallization (DRX) were investigated by optical microscope (OM), scanning electrical microscope (SEM), and electron backscattered diffraction (EBSD). Results show that the critical stress and strain for the initiation of DRX are determined from the work hardening rate curves. The volume fraction of DRX grains increases with increasing the temperature and strain. Both discontinuous dynamic recrystallization (DDRX) and continuous dynamic recrystallization (CDRX) coexist at low deformation temperature and low strain. The effect of CDRX becomes weaker with increasing the deformation temperature, and DDRX is the dominant nucleation mechanisms of DRX at higher temperatures. With increasing strain, the effect of DDRX becomes stronger, and CDRX can only be considered as an assistant nucleation mechanism of DRX at the latter stage of deformation for the studied superalloy. Additionally, Σ3 twin boundary contributes to the nucleation of DRX grains.

Key words: Ni-based superalloy; hot deformation characteristic; DRX behavior; nucleation mechanism of DRX

Ni-based superalloys generally have high hot processing resistance and a narrow hot processing window[1–3]. It is known that the hot components are prepared by hot deformation. During hot deformation, the evolution of microstructure is associated with the work hardening (WH), dynamic recovery and dynamic recrystallization (DRX) [4–6]. Simulation and experimental results show that DRX is a major softening mechanism of superalloys during hot deformation[7–10]. Moreover, DRX is also an effective way to refine the grain size and reduce the thermal processing resistance, so the mechanical properties are improved[11–13]. Consequently, it is essential to understand the DRX behavior of superalloys. The mechanisms of DRX mainly include: discontinuous DRX (DDRX) and continuous DRX (CDRX)[14–15]. DDRX involves the nucleation of new grains and subsequent grain growth[16]. The nucleation of DDRX is induced by the bulging of initial grain boundaries. The DDRX nuclei grow by the migration of grain boundaries. CDRX is realized through the progressive sub-grain rotation and geometric DRX, which is related to the continuous absorption of dislocations, and the new grains will form[17]. For superalloys with a low or middle stacking fault energy (SFE), CDRX is considered as an assistant nucleation mechanism of DRX at the low temperature or earlier deformation stage, while DDRX conducts as a dominant mechanism at the latter deformation stage[4,7].

It is well known that γ' particle characteristics, including volume fraction, size, morphology and distribution, are crucial to the DRX behavior[18]. Thus, γ' particles exert significant effect on the control of the microstructures and mechanical properties of superalloys[19]. Generally, γ' particles can affect the nucleation and growth of DRX grains. On the one hand, the nucleation of DRX grains occurs at the γ' particles, mainly due to the particle-induced DRX, characterized by the formation of sub-grains accelerated by γ' particles hindering dislocations motion[20]. On the other hand, the γ' particles can significantly hinder the grain boundary migration and limit

Received date: May 10, 2022
Foundation item: National Key Research and Development Program of China (2017YFA0700703); National Natural Science Foundation of China (51661019, 92060102); Program for Major Projects of Science and Technology in Gansu Province (145RTSA004); Hongliu First-Class Discipline Construction Plan of Lanzhou University of Technology
Corresponding author: Ding Yutian, Ph. D., Professor, State Key Laboratory of Advanced Processing and Recycling of Non-ferrous Metals, Lanzhou University of Technology, Lanzhou 730050, P. R. China, E-mail: dingyutian@126.com

grain growth referred as Zener drag[21]. The coherent γ′ particles undergo complex transformation when encountering with the moving grain boundaries[22]. The coherently precipitated γ′ possesses lower γ/γ′ interface energy and thereby exerts higher Zener pinning force on moving grain boundaries. Furthermore, the coherent interfaces will lose their coherency and transform into incoherent ones after encountering with moving grain boundaries[18], which is accompanied by the rotation, dissolution, and re-precipitation of the γ′ particles[23]. The dissolution of γ′ particles leads to the coarsening of DRX grains, because of the weakening of the pinning force exerted by the γ' precipitates on the moving grain boundaries[24].

The addition of Co can significantly reduce the SFE of superalloys[25]. A low SFE can inhibit the cross-slip and non-planar dislocation structure and facilitate the tendency to twinning[26]. Recently, deformation twinning is considered as an effective way to improve the mechanical properties as the arrangement of atoms are mirror reflections on both sides of the boundary plane[27–28]. In addition, it has been reported that the evolution of twin boundaries is closely related to the deformation parameters[29], which also play an important role in the nucleation of DRX grains due to the lattice rotations in superalloys with low SFE[30]. Thus, it is necessary to study the evolution of twin boundaries during hot deformation. The electron backscattered diffraction (EBSD) technique provides the detailed information about the grain orientations. Therefore, EBSD is a powerful tool to investigate the evolution of microstructures and the nucleation mechanisms of DRX.

In this work, isothermal compression tests were carried out in the deformation temperature range of 1040–1120 °C and the strain range of 0.35–1.2 with a strain rate of 0.1 s^{-1}. The aim of the study was to investigate the microstructure evolution, as well as to clarify the nucleation mechanisms of DRX of the studied superalloy during the hot deformation. Moreover, particular attention was paid to the evolution of the twin boundary and the γ′ particles.

1 Experiment

The chemical composition (wt%) of the studied superalloy is as follows: Ni-19.5Co-16.5Cr-5W-2.5Al-2.5Ti-2.5Nb-0.02C. Cylindrical specimens with a diameter of 10 mm and a height of 15 mm were machined from the forged bar with a diameter of 150 mm. The specimens were solution treated at 1080 °C for 4 h followed by oil quenching before hot deformation, and the typical microstructures of the specimens are shown in Fig.1. It can be seen that the initial microstructure is composed of numerous equiaxed grains with random orientations, the grain size is about 293.2 μm, and the fraction of Σ3 twin boundaries is about 47.7% (Fig.1a and 1b). And the γ′ particles show a spherical shape with a small diameter of 31.9 nm mainly ranging from 22 nm to 42 nm and are uniformly distributed in the matrix (Fig.1c and 1d).

Hot compression tests were conducted with a Gleeble-3800 thermal simulation machine at the temperatures of 1040, 1060, 1080, 1100 and 1120 °C, and the strain rate of 0.1 s^{-1}. The reductions of the specimens at different temperatures were set to 0.35, 0.7 and 1.2. In order to minimize the friction between the specimen and the fixture, the tantalum foils were

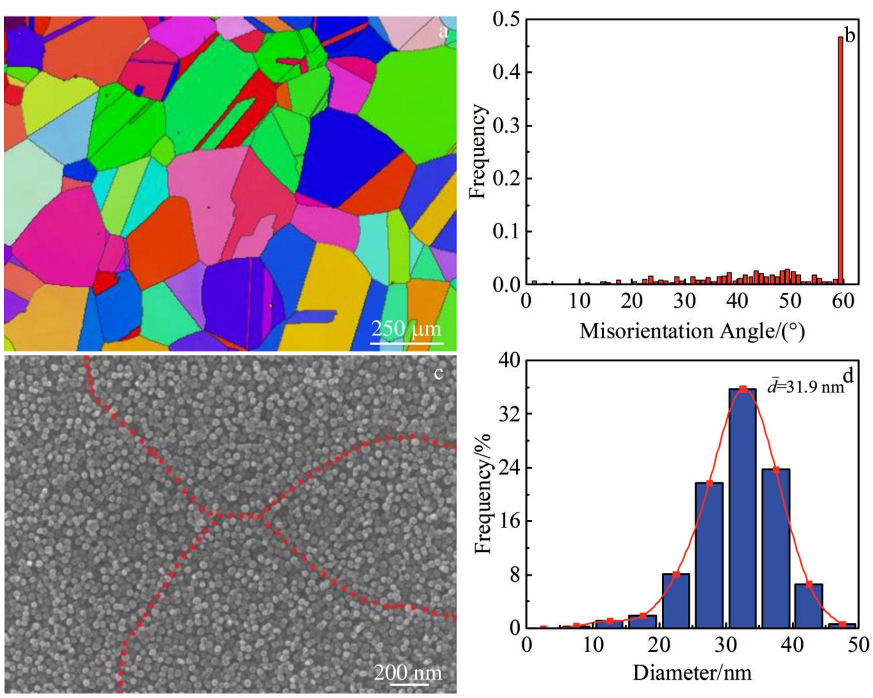

Fig.1 Typical initial microstructures of orientation imaging map (a), misorientation distribution (b), morphology of γ′ particles (c), and size distribution of γ′ particles (d) for the studied superalloy

placed on both ends of the specimens. A thermocouple was installed in the middle of the specimens to track the temperature change during the hot compression processes. Before hot compression, each specimen was heated to test temperature at a heating rate of 10 °C/s and held for 5 min to minimize the thermal gradients. During hot compression, the stress-strain data was automatically collected by the test system. After hot compression, the tested specimens were immediately quenched by water to maintain the deformed microstructures. Fig.2 shows the schematic diagram of the hot compression tests.

The deformed specimens were cut along the compression axis and then ground and mechanically polished. For optical microscope (OM) analysis, the mechanically polished specimens were etched in a solution consisting of $CuCl_2$ (5 g)+HCl (25 mL)+ethanol (25 mL) at room temperature for 2–3 min. For EBSD observations, the specimens were electron-polished in a chemical solution (80 mL methanol+20 mL H_2SO_4) at 20 V for 6–8 s. The specimens for SEM observations were electron-polished and then electro-chemically etched in a solution (15 g Cr_2O_3+10 mL H_2SO_4+150 mL H_3PO_4) at 4.5 V for 4–6 s.

2 Results and Discussion

2.1 Hot deformation characteristics

Fig. 3 shows the stress-strain curves of the superalloy at different testing temperatures. The flow stress curves exhibit three stages, i.e. an obvious work hardening stage followed by a softening stage and then a steady stage at the high strain zone. The shape of the flow stress curves indicates that the studied superalloy exhibits DRX features[31]. In the initial stage, the dislocations continuously appear and accumulate, resulting in the work hardening. And the dynamic recovery induced by dislocation cross-slip and climb is hardly to fully offset the work hardening[32]. Thus, the flow stress increases with the increase in strain. In the softening stage, the DRX occurs when the stress reaches a threshold (σ_c). The effect of work hardening is partially offset by softening mechanisms related to the nucleation and growth of DRX grains, and thus

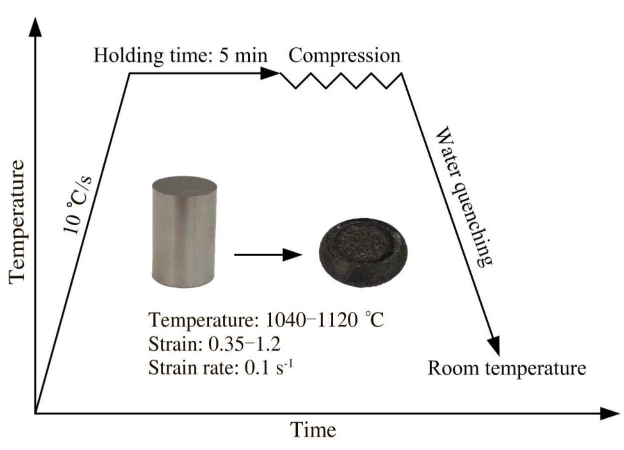

Fig.2 Schematic diagram of hot compression tests

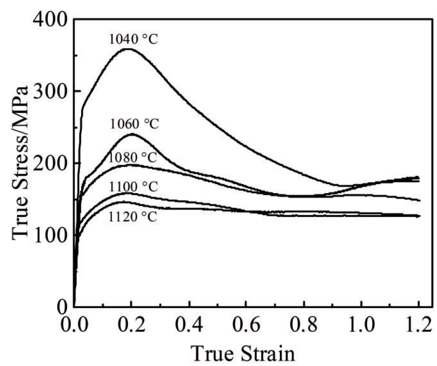

Fig.3 Stress-strain curves of specimens at different temperatures with a strain rate of 0.1 s^{-1}

work hardening rate is reduced. When the peak stress (σ_p) is reached, the DRX behavior is fully activated, and the softening effect exceeds the work hardening, which decreases the flow stress. Finally, a steady-state flow stress (σ_{ss}) can be obtained when the working hardening and dynamic softening reach a dynamic equilibrium.

Generally, DRX is initiated before the stress reaches σ_p. A thermodynamic method proposed by Poliakt and Jonass[33] can determine the critical stress for DRX (σ_c) and the critical strain (ε_c). In view of the thermodynamic theory, the critical value of DRX can be identified by the θ-σ curve, where θ is work hardening rate (θ=dσ/dε). The inflection point in the θ-σ curve represents the σ_c of DRX activated, which reflects the deformation mechanism variations[34]. The corresponding ε_c can be determined by the lnθ-σ curve. The critical points of σ_p and σ_{ss} can also be distinguished from the θ-σ curve.

Fig.4 shows the work hardening rate curves of the studied superalloy at different temperatures. The σ_c and ε_c for the occurrence of DRX are identified from the inflection point in the curves. It can be seen that the inflection points appear in the range where the strain is less than 0.14, which indicates that DRX is prone to occur at the tested temperatures. This may be due to small deformation degree to initiate DRX for superalloys at elevated temperatures[35]. After the inflection point, the value of θ quickly drops to zero with the flow stress reaching the σ_p, which is mainly caused by the increase in the DRX fraction. Moreover, although the steady state is not reached until an ultra-low stress at 1040 °C, the points of σ_{ss} can be traced in the θ-σ curves. This means that fully DRX can be achieved at high strain zone.

2.2 Microstructure characteristics

Fig. 5 shows the microstructures of the studied superalloy under different conditions. The fraction and morphology of DRX grains are significantly affected by the temperature and strain. At low temperature and strain, only a few DRX grains are nucleated at original grain boundaries. And in the high strain zone, the microstructure still includes a few elongated unrecrystallized grains. At high temperature and strain, DRX grains are obtained. As the deformation temperature exceeds 1080 °C, the fully DRX structures form at the latter stage of

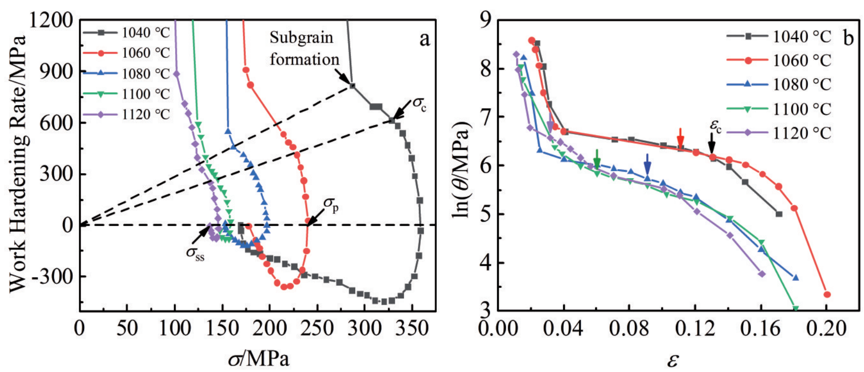

Fig.4 Change of work hardening rate with stress (a) and strain (b) of the studied superalloy at different temperatures

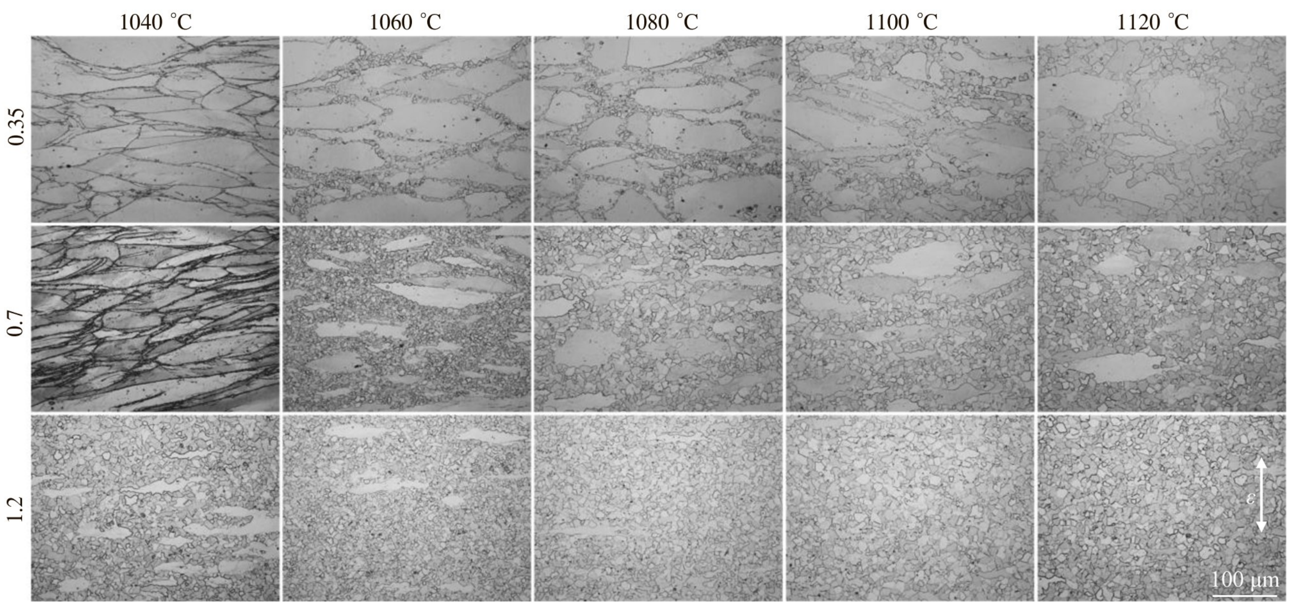

Fig.5 Microstructure characteristics of the studied superalloy at different deformation temperatures and strains

hot deformation.

2.3 Effect of deformation temperature on DRX

2.3.1 Microstructure evolution

To characterize the dependence of the grain structure and misorientations distribution with deformation temperature, some specimens were analyzed by EBSD technique. Fig. 6 shows the orientation imaging maps and the misorientation distribution of the studied superalloy at different temperatures. Different colors in the orientation imaging maps represent different grain orientations. At 1060 °C, the microstructure is mainly composed of elongated initial grains with sub-structure and some fully DRX grains. And the average misorientation angle is determined as 22.90° (Fig.6a and 6d). With increasing the temperature, the initial grains are gradually replaced by DRX grains, resulting in the decreased fraction of deformed and sub-structured grains. Meanwhile, the average misorientation angle increases to 23.02°, which also indicates that the amount of DRX grains increases with increasing the temperature (Fig. 6b and 6e). As the temperature increases to 1120 °C, numerous uniform and fine grains form accompanied by rapid reduction of sub-structured and deformed grains, especially the deformed grains which almost entirely disappear. The average misorientation angle further increases to 31.16° (Fig. 6e and 6f). This is because DRX is a thermal activation process, which involves the nucleation and growth of DRX grains. The DRX grain nucleation is related to the generation, accumulation and interaction of dislocations[36]. And the growth of DRX grains is mainly caused by the motion of grain boundary. The driving force for dislocation evolution and grain boundary migration increases with increasing the temperature, thereby promoting the DRX process. In addition, it can be seen that the fraction of Σ3 twin boundary increases with increasing the temperature, as shown in Fig. 6. The formation of Σ3 twin boundary can increase the mobility of grain boundary and accelerate the bulging and separation of serrated initial grains[37–38]. Thus, the nucleation of DRX can also be activated by the formation of Σ3 twin boundary.

Meanwhile, the precipitation and dissolution of γ' particles also have an important effect on the DRX behavior during hot

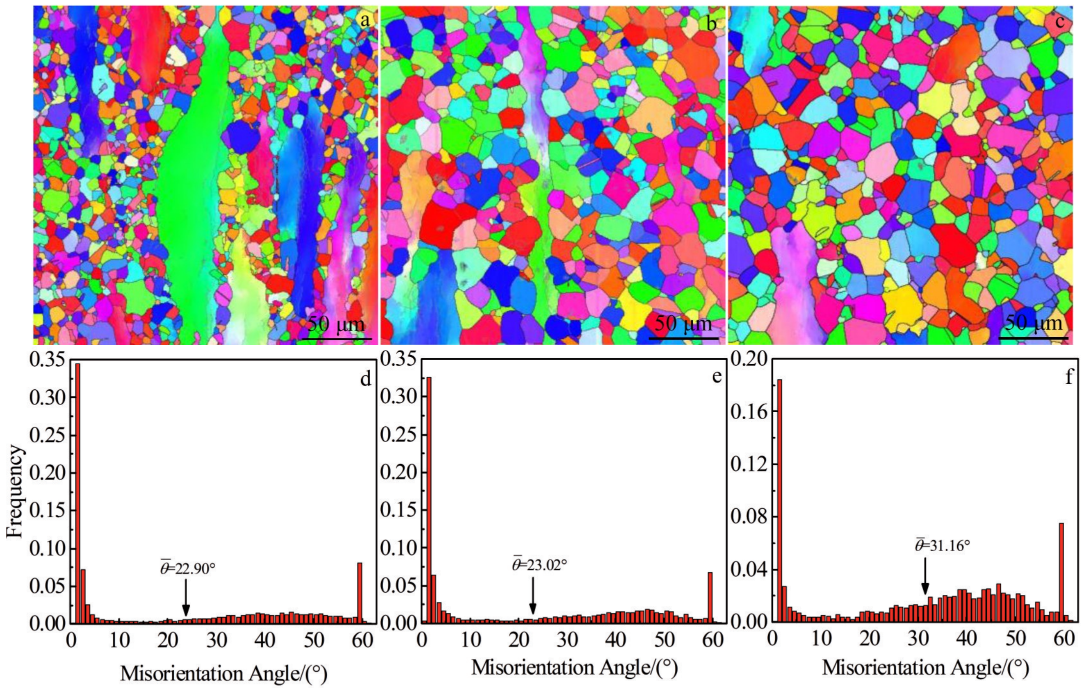

Fig.6 Orientation imaging maps (a–c) and misorientation distributions (d–f) of the studied superalloy at different temperatures with strain of 0.7: (a, d) 1060 °C, (b, e) 1100 °C, (c, f) 1120 °C

deformation. Fig. 7 shows the morphology and size of γ' particles in the deformed regions and the DRX regions of the studied superalloy at different temperatures. At 1060 °C, the coarse γ' particles preferentially transverse to the compression axis in the deformed regions (Fig. 7a), which is classified as type N (normal) coarsening[39]. The size of large γ' particles ranges from 55 nm to 90 nm and the average size is about 66.1 nm (Fig.7e). This is because the dislocations act as high-diffusivity paths to promote the diffusion of the γ'-forming elements, which in turn causes type N coarsening of γ' particles[40]. And the γ' particles facilitate the nucleation of DRX and the formation of new DRX grains as well[41]. Most of γ' particles seem to dissolve in DRX regions (Fig.7b) and the size becomes uniform with an average size of 32.2 nm (Fig. 7f). Coherent γ' particles in the matrix will lose their coherency after encountering the moving grain boundaries during DRX process[18]. With increasing the temperature, the size and distribution of γ' particles in DRX region do not significantly change (Fig. 7c and 7d, 7g and 7h), indicating that the γ' particles are stable when completing recrystallization. The stable γ' particles can efficiently inhibit the grain boundary migration and DRX grain growth, which is beneficial to the formation of the fine equiaxed grains at higher temperatures (Fig.6b and 6c).

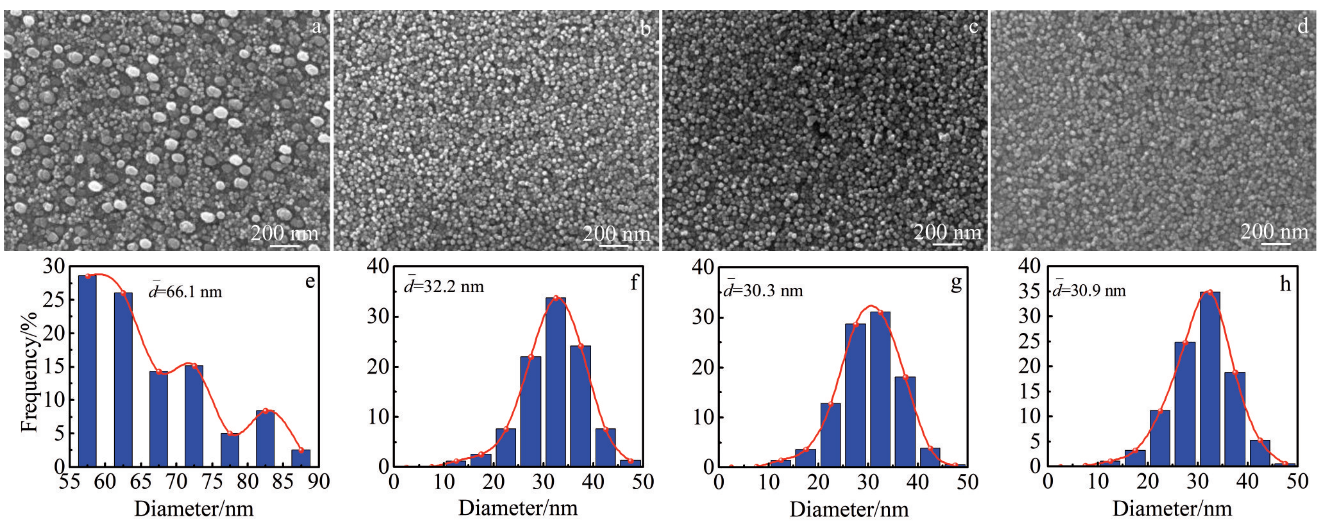

Fig.7 Morphology and size of γ' particles of the studied superalloy at strain of 0.7: (a, e) 1060 °C, DRX region; (b, f) 1060 °C, deformed region; (c, g) 1100 °C, deformed region; (d, h) 1120 °C, deformed region

2.3.2 Effect of deformation temperature on nucleation mechanisms of DRX

Fig. 8 shows the grain boundary maps of the specimens at different temperatures. The Σ3 boundaries (<111> 60°) are represented by red lines. The low angle grain boundaries (LAGBs) with misorientations θ<10° are represented by gray lines, the high angle grain boundaries (HAGBs) with θ>15° are black lines. The grain boundaries with misorientations between 10° and 15° are defined as middle angle grain boundaries (MAGBs), which are represented by green lines. At 1060 °C, HAGBs are extensively formed at the serrated and bulged grain boundaries which are the typical characteristics of DDRX. Moreover, some LAGBs can also be observed along the elongated initial grain boundaries, which suggest the occurrence of CDRX (Fig. 8a). This indicates that the mechanisms of DDRX and CDRX simultaneously exist at the low temperature. At 1100 °C, the number of sub-structured grains with LAGBs decreases, indicating that the effect of CDRX becomes weaker (Fig. 8b). In other words, the DDRX nucleation mechanism is promoted at the temperature of 1100 °C. As the deformation temperature reaches 1120 °C, most of the grain boundaries are HAGBs and only few grains with sub-structure can be observed (Fig. 8c), indicating that DDRX is the dominant mechanism at the high temperature.

The CDRX is realized by progressive rotation of sub-grains which can be evaluated by the development of misorientation angle (orientation gradient) along the sub-structured grain boundaries and within the sub-grains [32]. And 10°–15° angles indicate the occurrence of CDRX in sub-grains. To understand the effect of deformation temperature on the misorientation angles, the point to point (local) misorientation and point to origin (cumulative) misorientation are presented along the lines marked in Fig. 8. The local misorientation cannot exceed 3° both along the sub-grain boundaries and within the grains, while the cumulative misorientation can exceed 10° (Fig. 9a and 9b), indicating that CDRX has been well developed at 1060 °C. Moreover, the orientation gradient along the initial grain boundaries is greater than that of the grains interior, indicating that the nuclei easily transform to the HAGBs[2]. The cumulative misorientations along the line B1 and B2 decrease with the increase in temperature, (Fig. 9c and 9d). This indicates weakened effect of progressive sub-grain rotation and the accelerated sub-grains transformed from LAGBs to HAGBs. As the temperature increases to 1120 °C, the level of cumulative misorientation further decreases and cannot exceed 8° (Fig.9e and 9f), indicating that CDRX effect is significantly weakened at the higher temperature.

2.4 Effect of strain on DRX

2.4.1 Microstructure evolution

Fig. 10 shows the orientation imaging maps and the plots of misorientation distribution of the studied superalloy. The microstructure is significantly influenced by strain. At the strain of 0.35, the structure is composed of a large number of sub-structured grains and only a small amount of DRX grains (Fig. 10a). However, the initial grain boundary becomes serrated, which facilitates the nucleation of DRX grains through grain boundary bulging. As the strain increases to 0.7, the initial grains gradually disappear and DRX grains form at the bulged grain boundary (Fig. 10b). Generally, it is accepted that grain boundary bulging is related to strain-induced grain migration, which is driven by different orientations of adjacent grains [7]. Moreover, the stored energy increases with increasing the strain, resulting in the increased driving force for grain boundary migration [3], and thereby the degree of DRX can be accelerated by straining. As the strain reaches to 1.2, the complete dynamic recrystallization occurs, i. e., the equiaxed grains with an average size of about 6 μm are prevalent. Meanwhile, a certain number of Σ3 twin boundaries are also found in the newly recrystallized grains (Fig. 10c). In addition, the average misorientation angles at the strains of 0.35, 0.7 and 1.2 can be determined as 11.12°, 21.77° and 30.23°, respectively (Fig. 10d–10f). The increasing average misorientation angle is affected by the growth of DRX nuclei, which are related to the annihilation of dislocations [17]. This reveals the reason why the LAGBs induced by dislocation multiplication transform to the HAGBs associated with the increasing average misorientaion angles.

Fig. 11 shows the morphology and size distributions of γ'

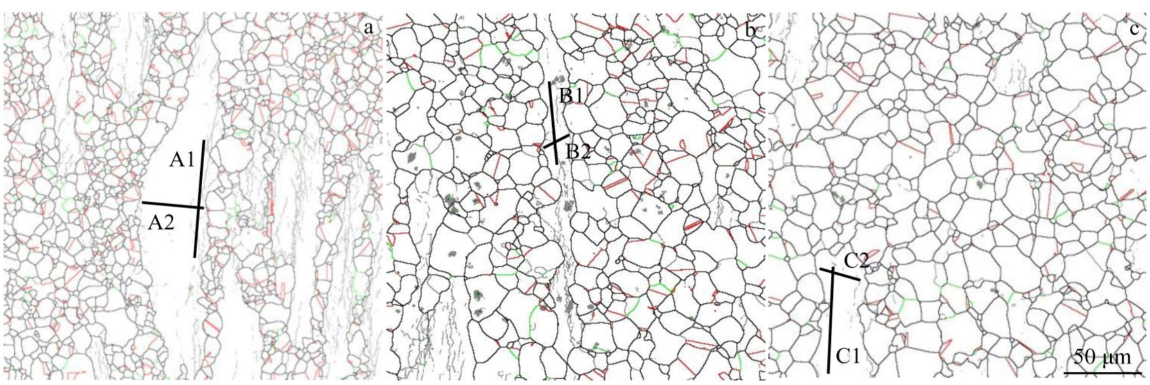

Fig.8 Grain boundary maps of the studied superalloy at the strain rate of 0.1 s^{-1} and strain of 0.7 at different temperatures: (a) 1060 °C, (b) 1100 °C, and (c) 1120 °C

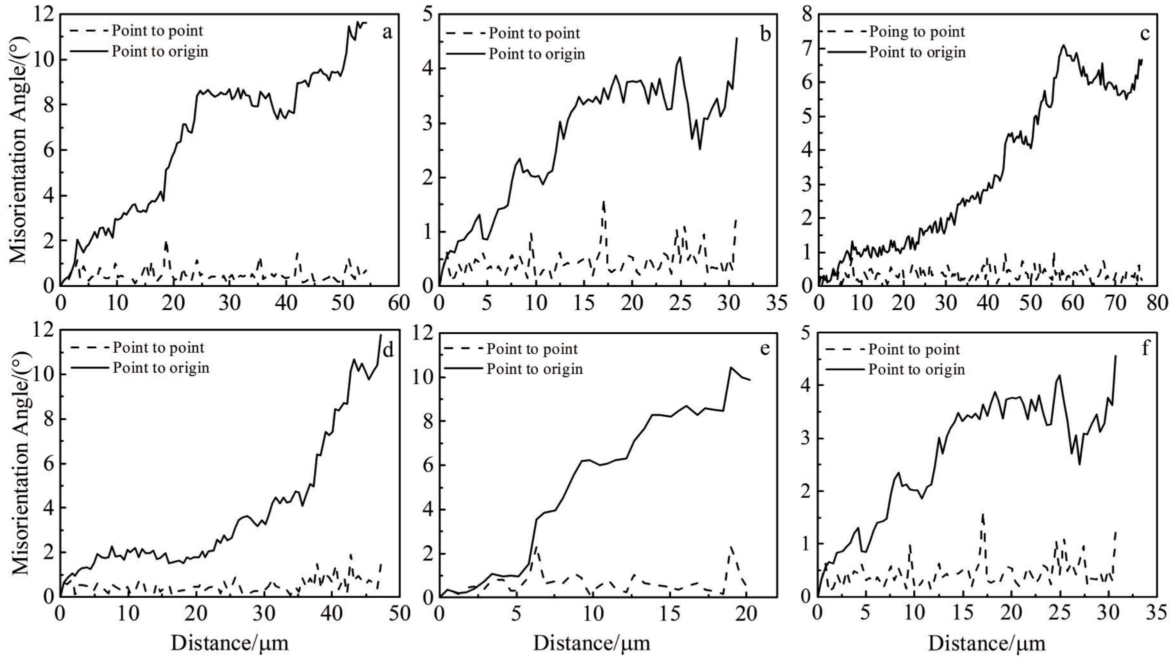

Fig.9 Misorientations measured along the lines marked in Fig.8: (a) A1, (b) A2, (c) B1, (d) B2, (e) C1, and (f) C2

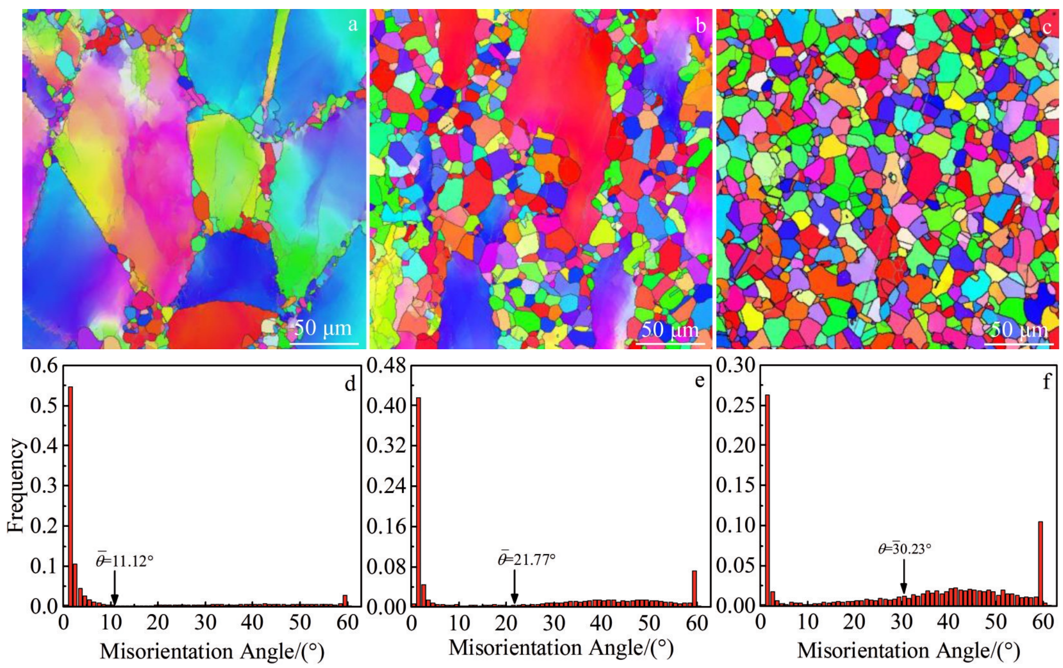

Fig.10 Orientation imaging maps (a–c) and misorientation distribution plots (d–f) of the studied superalloy at the strain rate of 0.1 s^{-1} and deformation temperatures of 1080 °C with different strains: (a, d) 0.35, (b, e) 0.7, and (c, f) 1.2

particles in DRX regions of the studied superalloy at different strains. A large number of spherical γ' particles are uniformly distributed at the matrix and grain boundaries (Fig. 11a). Meanwhile, the size of γ' particles with an average diameter of 27.4 nm mainly ranges from 18 nm to 37 nm (Fig.11d). With increasing the strain, the size of γ' particles gradually increases to 37.6 nm (Fig.11e), especially the γ' coarsening at the grain boundaries is more obvious (Fig. 11b). And thus, the γ' particles exert enhanced pinning effect on the DRX grains, which limits the grain growth[40]. At the latter stage, the γ' particles inside of the grains are not significantly coarsened (Fig.11f), but the number of γ' particles at the grain boundaries further increases (Fig. 12c), suggesting that the hindering effect of γ' on DRX grain boundary migration becomes stronger. This is an important factor for the formation of uniform fine grains when deformed at 1080 °C (Fig.10c).

2.4.2 Effect of strain on nucleation mechanisms of DRX

In order to reveal the effect of strain on the nucleation

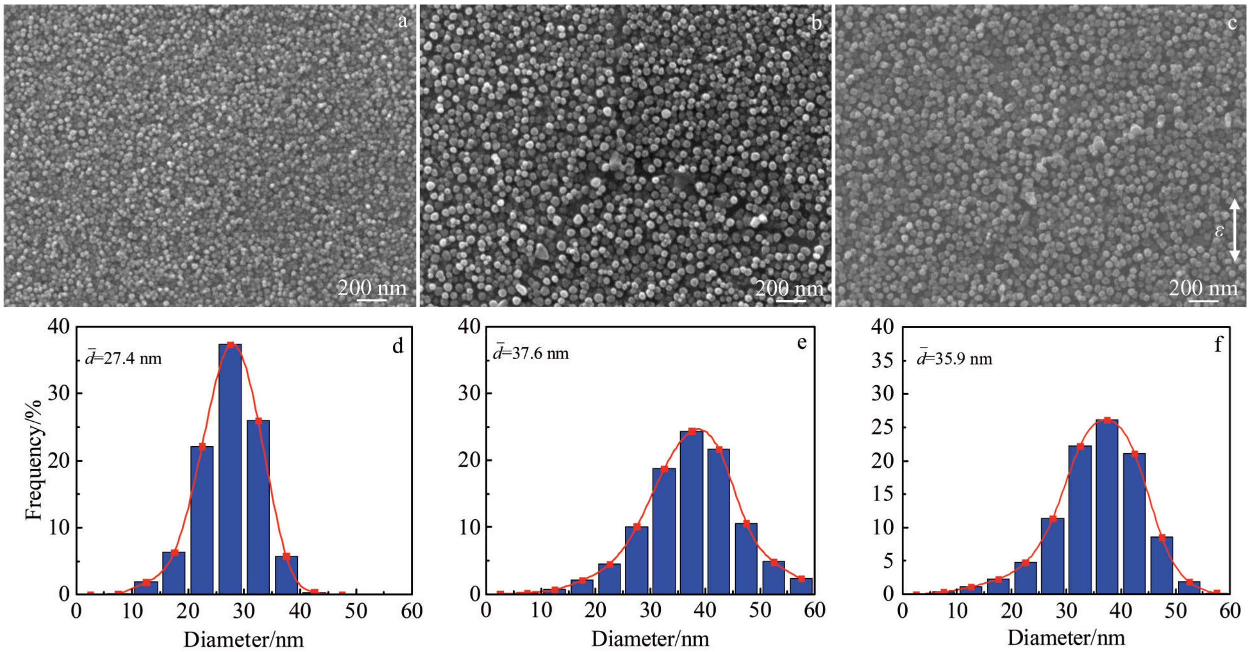

Fig.11 Morphologies (a–c) and size distributions (d–f) of γ' particles of the studied superalloy deformed at 1080 °C in DRX region with different strains: (a, d) 0.35; (b, e) 0.7; (c, f) 1.2

mechanism of DRX, the grain boundary maps of the studied superalloy under different strains are shown in Fig.12. At the earlier deformation stage, some HAGBs occuring at the bulged grain boundary induced by boundary migration can be observed, which is the feature of DDRX. Moreover, sub-grains with LAGBs also form near the initial grain boundaries (Fig.12a), indicating the occurrence of CDRX. Thus, DDRX and CDRX also occur simultaneously at the earlier stage of deformation. With increasing the strain, a growing number of LAGBs are transformed into HAGBs along the initial grain boundaries, indicating that the effect of DDRX becomes more obvious (Fig. 12b). When the strain increases to 1.2, the number of HAGBs increases significantly and that of LAGBs decreases (Fig.12c). This indicates that the effect of CDRX is weakened at the latter stage of deformation.

Fig. 13 shows the local misorientations and cumulative misorientations along the lines marked in Fig. 12. It is obvious that either near the initial grain boundaries or within the grains, the cumulative misorientations cannot exceed 8° (Fig.13a and 13b), indicating that the effect of progressive sub-grain rotation is not obviously manifested at the earlier deformation stage. As the strain reaches 0.7, the cumulative misorientations along the initial boundaries can exceed 10° (Fig. 13c and 13d), implying that the progressive sub-grain rotation becomes stronger with increasing the strain. When the strain increases to 1.2, the cumulative misorientations significantly decrease and can hardly exceed 1° (Fig.13e and 13f), suggesting that the effect of the CDRX is weakened. Therefore, the effect of progressive sub-grain rotation can only be considered as an assistant nucleation mechanism of DRX for the superalloy at the latter stage of deformation.

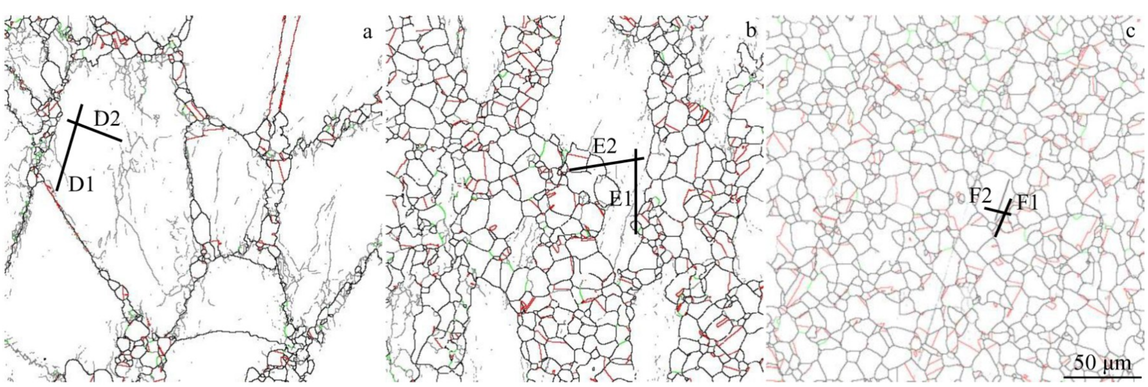

Fig.12 Grain boundary maps of the studied superalloy at deformation temperature of 1080 °C with different strains: (a) 0.35, (b) 0.7, and (c) 1.2

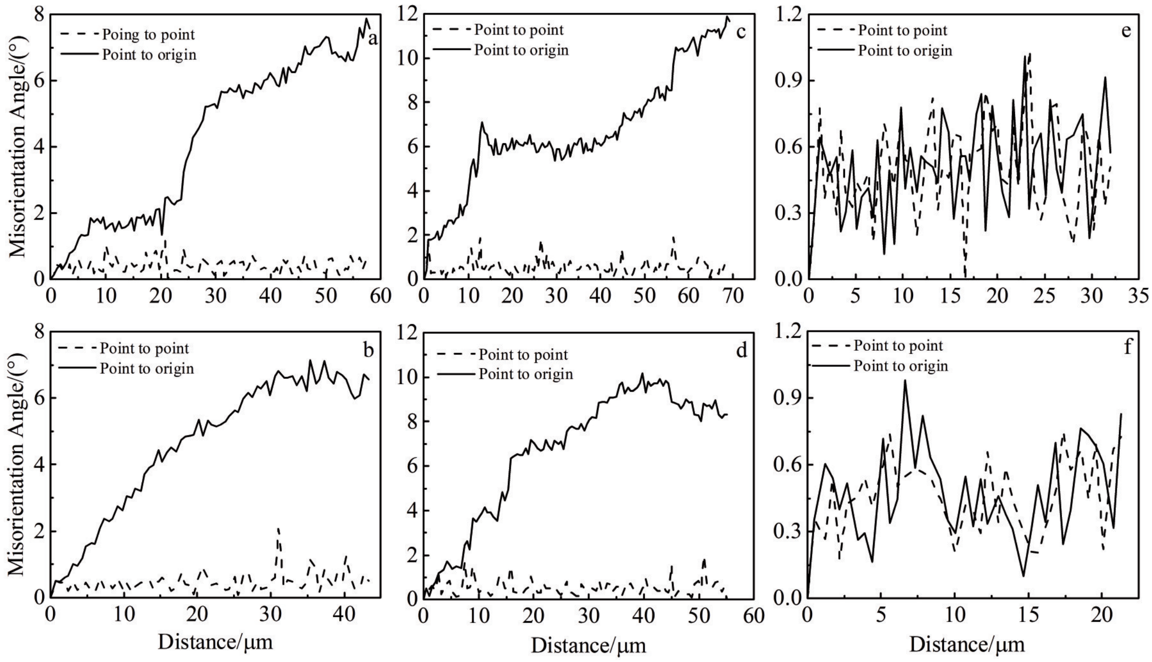

Fig.13 Misorientations measured along the lines marked in Fig.12: (a) D1, (b) D2, (c) E1, (d) E2, (e) F1, and (f) F2

3 Conclusions

1) The critical stress and strain for the initiation of DRX can be determined from the work hardening rate curves. And the fully DRX can be achieved at the high strain zone.

2) The DRX behavior is significantly influenced by the temperature and strain. The volume fraction of DRX grains increases with increasing the temperature and strain, which is related to the transition from LAGBs to HAGBs.

3) The mechanism of DDRX and CDRX coexists at the low deformation temperature and strain. The effect of CDRX characterized by progressive sub-grain rotation becomes weaker with increasing the temperature, and DDRX is the dominant nucleation mechanism of DRX at higher temperatures. With increasing the strain, the effect of DDRX becomes stronger, and CDRX can only be considered as an assistant nucleation mechanism of DRX at the latter stage of deformation of the studied superalloy.

4) At the low temperatures, coarse γ' particles preferentially transverse to the compression axis in deformed regions and most of the γ' particles dissolve in DRX regions. The size of γ' particles increases with the increase in strain, especially the γ' coarsening at the grain boundaries which is more obvious. The γ' particles are beneficial to the formation of uniform and fine equiaxed grains.

5) With increasing the deformation temperature and strain, the fraction of Σ3 boundaries increases. The nucleation of DRX can be activated by the formation of Σ3 boundaries, which can increase the grain boundary mobility and accelerate the bulging and separation of serrated initial grains.

References

1 Chen X M, Lin Y C, Wen D X *et al. Materials and Design*[J], 2014, 57(5): 568

2 Lin Y C, He D G, Chen M C *et al. Materials and Design*[J], 2016, 97: 13

3 Zhang C, Zhang L W, Shen W F *et al. Journal of Alloys and Compounds*[J], 2017, 728: 1269

4 Zhang H B, Zhang K F, Jiang S S *et al. Journal of Alloys and Compounds*[J], 2015, 623: 374

5 Kong Y H, Chang P P, Li Q *et al. Journal of Alloys and Compounds*[J], 2015, 622: 738

6 Zhang L, Wang W, Shahzad M B *et al. Acta Metallurgica Sinica*[J], 2019, 32(9): 1161

7 Li D F, Guo Q M, Guo S L *et al. Materials and Design*[J], 2011, 32(2): 696

8 Ouyang L X, Luo R, Gui Y W *et al. Materials Science and Engineering A*[J], 2020, 788: 139 638

9 Chen F, Cui Z S, Ou H A *et al. Applied Physics A*[J], 2016, 122(10): 890

10 Zhang C, Tang X L, Zhang L W *et al. Journal of Materials Research*[J], 2019, 34(18): 1

11 Qu J L, Xie X F, Bi Z N *et al. Journal of Alloys and Compounds*[J], 2019, 785: 918

12 Wang Y, Shao W Z, Zhen L *et al. Materials Science and Engineering A*[J], 2008, 486: 321

13 Zhang P, Hu C, Zhu Q *et al. Materials and Design*[J], 2015, 65: 1153

14 Wang Y, Shao W Z, Zhen L *et al. Materials Science and Engineering A*[J], 2008, 497(1-2): 479

15 Mehtonen S V, Karjalainen L P, Porter D A. *Materials Science and Engineering A*[J], 2013, 571: 1

16 Wu H, Liu M X, Wang Y *et al. Journal of Materials Research*

and Technology[J], 2020, 9(3): 5090
17 Yu C, Di H S, Zhang J Q *et al. Materials Science and Engineering A*[J], 2013, 585: 71
18 Zhou X, Ma T F, Li Y L *et al. Materials Science and Engineering A*[J], 2019, 761: 138 046
19 Vernier S, Franchet J M, Dumont C *et al. Metallurgical and Materials Transactions A*[J], 2018, 49(9): 4308
20 Lv S M, Jia C L, He X B *et al. Advanced Engineering Materials*[J], 2020, 22(12): 1
21 Zhang C, Zhang L W, Li M F *et al. Journal of Materials Research*[J], 2014, 29(23): 2799
22 Song K, Aindow M. *Materials Science and Engineering A*[J], 2007, 479(1): 365
23 Lu Q, Pei Y L, Li S S *et al. Materials and Design*[J], 2017, 130: 69
24 Monajati H, Jahazi M, Bahrami R *et al. Materials Science and Engineering A*[J], 2004, 373: 286
25 Shang S L, Zacherl C L, Fang H Z *et al. Journal of Physics Condensed Matter*[J], 2012, 24(50): 505 403
26 Yuan Y, Gu Y F, Cui C Y *et al. Journal of Materials Research*[J], 2011, 26(22): 2833
27 Lu K, Lu L, Suresh S. *Science*[J], 2009, 324(5925): 349
28 Lu L, Shen Y F, Chen X H *et al. Science*[J], 2004, 304: 422
29 Jia Z, Gao Z X, Ji J J *et al. Advanced Engineering Materials*[J], 2019, 21(9): 190 0426
30 Wang X, Brünger E, Gottstein G *et al. Scripta Materialia*[J], 2002, 46(12): 875
31 Zhang H B, Zhang K F, Jiang S S *et al. Journal of Materials Research*[J], 2015, 30(7): 1029
32 Lin Y C, Wu X Y, Chen X M *et al. Journal of Alloys and Compounds*[J], 2015, 640: 101
33 Poliakt E I, Jonass J J. *Acta Materialia*[J], 1996, 44(1): 127
34 Chen M S, Lin Y C, Ma X S. *Materials Science and Engineering A*[J], 2012, 556: 260
35 Lin Y C, Chen X M, Wen D X *et al. Computational Materials Science*[J], 2014, 83: 282
36 Lin Y C, Liu Y X, Chen M S *et al. Materials and Design*[J], 2016, 99: 107
37 Wan Z P, Wang T, Sun Y *et al. Acta Metallurgica Sinica*[J], 2019, 55(1): 45 (in Chinese)
38 Gottstein G. *Acta Metallurgica*[J], 1984, 32(7): 1117
39 Véron M, Bréchet Y, Louchet F. *Acta Materialia*[J], 1996, 44(9): 3633
40 Seret A, Moussa C, Bernacki M *et al. Metallurgical and Materials Transactions A*[J], 2018, 49(9): 4199
41 Ning Y Q, Yao Z K, Guo H Z *et al. Materials Science and Engineering A*[J], 2010, 527(26): 6794

一种新型镍基高温合金的动态再结晶行为

王兴茂[1,2]，丁雨田[1]，毕中南[2]，于鸿垚[2]，杜金辉[2]，甘　斌[2]
(1. 兰州理工大学 省部共建有色金属先进加工与再利用国家重点实验室，甘肃 兰州 730050)
(2. 钢铁研究总院 高温合金新材料北京市重点实验室，北京 100081)

摘　要：采用等温热压缩实验研究了一种新型镍基高温合金在不同热变形条件下（变形温度1040~1120 ℃、应变量0.35~1.2、应变速率0.1 s^{-1}）的动态再结晶行为。通过光学显微镜（OM）、扫描电子显微镜（SEM）和电子背散射衍射仪（EBSD）研究变形温度和应变量对合金热变形过程中组织演变和动态再结晶（DRX）形核机制的影响。结果表明，根据加工硬化率曲线能够准确确定DRX出现的临界应力和临界应变。合金的DRX晶粒体积分数随变形温度和应变量的增加而增加。在高温低应变速率下，不连续动态再结晶（DDRX）和连续动态再结晶（CDRX）形核机制同时发生。随着变形温度的升高，CDRX形核机制减弱，而CDRX机制在高温条件下占据主导。随着应变量的增加，合金中DDRX机制逐渐变强。热变形后期，CDRX仅作为辅助形核机制发挥作用。另外，Σ3孪晶界的形成有助于DRX晶粒的形核。

关键词：镍基高温合金；热变形特征；动态再结晶行为；形核机制

作者简介：王兴茂，男，1994年生，博士生，兰州理工大学省部共建有色金属先进加工与再利用国家重点实验室，甘肃 兰州 730050， E-mail：wangxingmao9818@163.com